Understanding the critical role of boundary conditions in meso-scale finite element simulation of braided composites

(Article begins on next page)

**BRIEF COMMUNICATION**

# Understanding the critical role of boundary conditions in meso-scale finite element simulation of braided composites

Zhenqiang Zhao[1,2,3] · Peng Liu[1,2] · Haoyuan Dang[1,2] · Yang Chen[4] · Chao Zhang[1,2,4] · Alfonso Pagani[5]

## Abstract

A reasonable boundary condition for the meso-scale finite element (FE) simulation of textile composites is necessary for model validation against experiments, which is sometimes over-simplified for saving computation time. This paper examines the influence of boundary conditions on the global stress–strain response and deformation pattern, as well as the local damage and failure characters, through systematically comparison studies of numerical results against experimental results under different loading conditions. The results suggest that reasonable application of periodic boundary conditions can effectively improve the calculation efficiency, and the employment of symmetric boundary conditions along the loading direction will cause the undesired strain concentration and premature damage at the loading edges of the model. Besides, extra constraints along the thickness direction may restrain the normal out-of-plane deformation of the braided composites and thereby cause an overestimation of the transverse strengths.

**Keywords** Braided composites · Meso-scale model · Boundary condition · Free-edge effect · Progressive failure simulation

## 1 Introduction

The textile composites have been widely used in the fields of aerospace, automotive, marine, etc., due to their superior mechanical performance and suitability for integrated molding of the complex structures [1, 2], as well as their potential applications in the fields of electromagnetic and intelligent materials [3–6]. However, its intricate braided architecture and sometimes large size in the representative unit cell (UC) leads to a complex deformation and failure behavior [7, 8], which drives the meso-scale finite element

simulation to become a popular method in relevant analysis and prediction [9–13]. Nevertheless, the implementation of the meso-scale simulation for the textile composites is time-consuming attribute to the fictitious reconstruction of the braided architecture and model individually the deformation and failure process of each component of the braided composites. As a result, the meso-scale simulation is usually performed on the periodic UC which is much smaller in size than the experimental samples but can represent the composite's geometric features and mechanical performance.

During a simulation scenario, the comparability between the small size UC model and the large size specimen is relying on the reasonable application of boundary conditions. The uniform strain or stress boundary conditions were easier applied on a single RVE model to calculate the homogenized mechanical properties, such as the works presented in [14–17]. Also, some researchers utilized the symmetric boundary condition (SYBC) [18, 19] or other local constraints [20–23] in the RVE model to predict the mechanical behavior of a sample contains multiple UCs in-plane or through-the-thickness. Besides, the periodic boundary conditions (PBC) [24] are also employed frequently to model the mechanical behavior of the continuous fiber-reinforced [25–32] and

✉ Chao Zhang
  chaozhang@nwpu.edu.cn

1 School of Aeronautics, Northwestern Polytechnical University, Xi'an 710072, Shaanxi, China

2 Joint International Research Laboratory of Impact Dynamics and Its Engineering Applications, Xi'an 710072, Shaanxi, China

3 School of Science, Harbin Institute of Technology, Shenzhen 518055, Guangdong, China

4 School of Civil Aviation, Northwestern Polytechnical University, Taicang 215400, Jiangsu, China

5 Department of Mechanical and Aerospace Engineering, Politecnico Di Torino, 10129 Torino, Italy

the particle or discontinuous fiber-reinforced composites [24, 33–35]. In practice, different boundary conditions are usually used in combination. Barbero et al. [36] assigned the SYBC and the uniform strain constraint to one-quarter of the UC to predict the elastic and in-elastic behaviors of a plain weave composite. Jiang et al. [37] employed the PBC in conjunction with the SYBC to simulate the failure behavior of a triaxially braided composite under tensile load, the method of which will be further investigated in this study.

A lot of experimental [38, 39] and numerical [40, 41] results reveal that mechanical performances of braided composites exhibit high sensitivity to the sample size and the applied boundary conditions, which can be attributed to their large size in UC. Hence, it is no doubt that the reasonability of the boundary condition plays a critical role in predicting the mechanical response and failure behavior of composite material [42]. Unfortunately, this issue was ignored or skipped in most of the related publications. Rare works reported by Song [43] and Zhang et al. [44] only concerned with the usage and effectiveness of the PBC on the UC of braided composites. In this study, the two-dimensional triaxially braided composite (2DTBC) is taken as an example to investigate systematically the influence of boundary conditions and model size on the meso-scale simulation results. Then the more effective method of boundary condition definition is proposed in a view of the numerical model validation, which can provide an important reference for the further development of mesoscopic FE simulation of textile composites.

## 2 Meso-scale FE model and boundary conditions

### 2.1 Model generation of 2DTBC

The meso-scale FE method is mature in simulating the mechanical behaviors of braided composites. The main focus of this study is the usability of boundary conditions when employing the meso-scale simulation, and the detail of generating the meso-scale FE model as well as the constitutive model for each component of the 2DTBC can be found in previous studies [11, 39, 40]. During the simulation, the impregnated fiber tows are modeled as a transversely-isotropic material in which the Hashin-based damage criterion [45] is employed in cooperating with the Murakami-Ohno damage theory [46] to simulate the internal damage initiation and evolution. The pure matrix

part is modeled as an elastic–perfectly plastic material. Besides, a cohesive element model [31] is employed to simulate the tow-to-tow and tow-to-matrix delamination. It is worthy to note that the FE models of 2DTBC adopted in this study have been extensively validated in previous works [39, 40].

### 2.2 Definition of boundary conditions

In Fig. 1, the different boundary conditions are applied individually or cooperatively on the meso-scale FE models with different dimensions, aiming to simulate the mechanical responses of the 2DTBC coupon specimen under axial tension (AT), transverse tension (TT), axial compression (AC), and transverse compression (TC). For the AT or TT condition, as shown in Fig. 1a, b, the full-width 8-layer FE model matching the tested specimen was adopted, and the PBC or the combined uniform displacement (UD) with SYBC (denoted as UDSYBC) is used in the loading direction to simulate the long gauge section of the specimen. Also, the half-width FE model was also employed in conjunction with the SYBC to simulate the full-width specimen, and the UDSYBC or PSYBC (PBC combined with SYBC [37]) was applied in the loading direction. The AC and TC tests were also simulated by the full width or half width FE models, as shown in Fig. 1c, d. For one of the full-width models making use of UDBC, two elastic bodies are placed on both sides of the gauge region to simulate the clamping compression condition for the compression specimens [47]. In contrast, the other full width model adopts the UDSYBC in the loading direction. The half width model and the applied boundary conditions for compression simulations were the same as those for tension simulations. The label of each model is attached to its schematic drawings in Fig. 1.

The computational efforts of the meso-scale simulation can be reduced by employing the SYBC on the thickness direction of the FE model, which has been implemented by Li et al. [48]. In Fig. 2, the model named "F-ZSYM" indicates that the SYBC was applied on the top surface of a full-width four-layer model, and the label "F-ZDSYM" signifies that two symmetric constraints were applied simultaneously to the upper and lower surfaces of a full-width two-layer model. The in-plane tensile and compressive loads will be imposed in the same way as those in F-PBC for tension simulation and F-UDBC for compression simulation, respectively. Also, single-layer models imposing a through-the-thickness PBC as reported in [40] are involved here as well to predict the mechanical response of the infinitely thick specimen (denoted as F-ZPBC model).
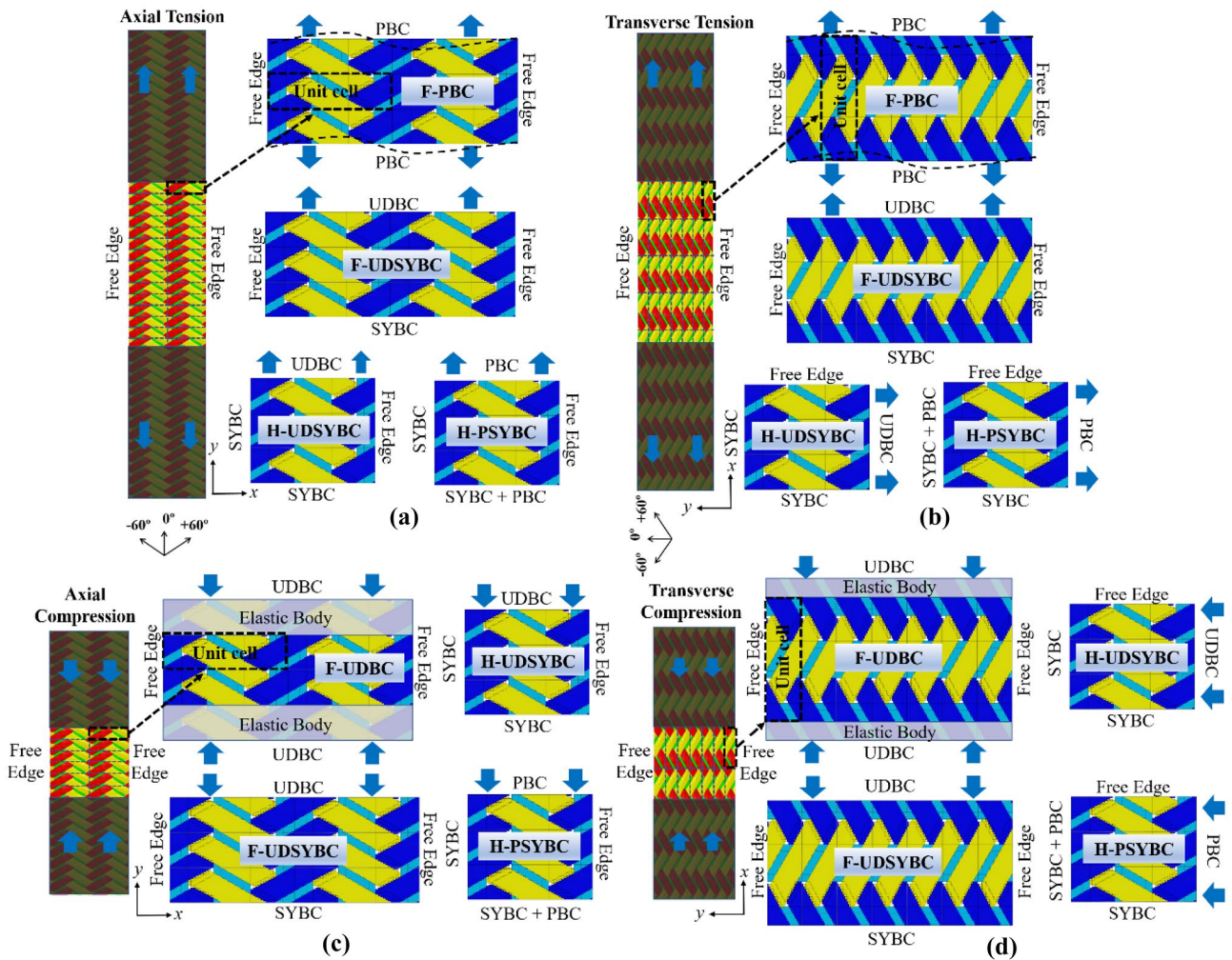
**Fig. 1** Meso-scale FE models with different in-plane boundary conditions for the simulation of **a** axial tension, **b** transverse tension, **c** axial compression, and **d** transverse compression

The method of applying each boundary condition aforementioned can be illustrated by Fig. 2, in which a FE model of 2DTBC is generated in a rectangular coordinate system and the monotonic load is hypothetically imposed along x-axis. As shown in the left half of Fig. 2, each face of the model is marked according to its normal direction, and the two opposite faces along the same axis are distinguished by assigning plus or minus after the capital letters X, Y, and Z, respectively. After that, the loading boundary conditions can be applied by activating the governing equations below:

Assuming that the UDBC is applied on $X+$ surface, then (Eq. 1),

$$u_x^{X+} = \delta_x \tag{1}$$

Assuming the SYBC is applied on $X-$ surface, then (Eq. 2),
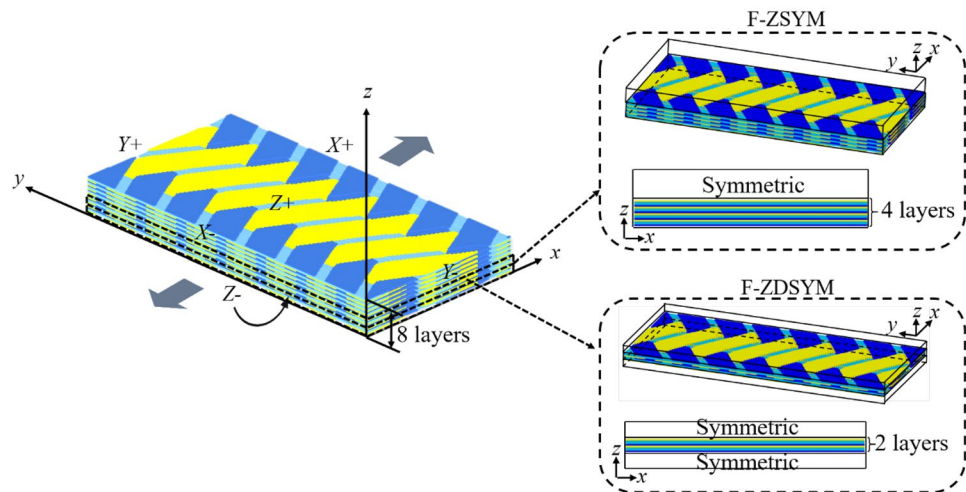
$$u_x^{X-} = 0 \tag{2}$$

Assuming the PBC is applied on opposite surfaces $X+$ and $X-$, then (Eq. 3),

$$\begin{cases} u_x^{X+} - u_x^{X-} = \delta_x \\ u_y^{X+} - u_y^{X-} = 0 \\ u_z^{X+} - u_z^{X-} = 0 \end{cases} \tag{3}$$

Finally, assuming that the PSYBC is applied on opposite surfaces $X+$ and $X-$, then (Eq. 4),

**Fig. 2** Schematic diagram of the transverse tensile models with different thicknesses



where $u$ represents the displacement variable and $\delta$ indicates the specified applied displacement; superscripts $X+$ and $X-$ denote the node-set on opposite surfaces of the model along $x$-axis, as shown in Fig. 2; and subscripts $x$, $y$, and $z$ refer to the three axes, respectively.

$$\begin{cases} u_x^{X+} = \delta_x \\ u_y^{X+} - u_y^{X-} = 0 \\ u_z^{X+} - u_z^{X-} = 0 \\ u_x^{X-} = 0 \end{cases} \qquad (4)$$

# 3 Results and discussions

## 3.1 Effect of in-plane B.C. on tensile simulation results

Figure 3 gives the numerical predictions of tensile responses from the meso-scale FE models depicted in Fig. 1a, b. The experimental results of the long coupon specimens of 2DTBC reported in Zhao et al. [47] are also presented here to evaluate the simulation results. From Fig. 3, we can see that the numerical predictions of stress–strain curves and strain distributions of AT from different models are comparable. On the other hand, the simulation results of TT depend on the boundary conditions adopted; the full-width models without using the SYBC as well as the H-PSYBC model predicted well the experimental results. The predicted transverse tensile response from the H-UDSYBC model and F-UDSYBC model present unnatural strain concentrations along the loading edge and significantly underestimate the

transverse strength, which does not agree with the experimental results.

Figure 4 shows the tensile damage patterns predicted by different FE models and the corresponding comparisons with the failure morphologies observed from the tested specimens. From the damage patterns shown in Fig. 4a, the fiber breakage in axial tows and matrix cracking among bias tows can be reasonably predicted by these four models. The studied boundary conditions although affect the deformation patterns, however, do not affect the loading path of the specimen, where the axial fiber bundles are still going across the two loading ends and play a major role in load affording. From the simulation results shown in Fig. 4b, we can find in the F-PBC and the H-PSYBC models that fiber damage goes across some bias fiber tows and the matrix damage is evenly distributed in both the axial and bias tows, which matches well with the experimental results. However, little fiber damage is observed in F-UDSYBC and H-UDSYBC models, and the predicted matrix damage is unreasonably centralized along the loading edges.

## 3.2 Effect of in-plane B.C. on compressive simulation results

For the simulation results of compression conditions, firstly, we can see in Fig. 5a, b that there is no significant difference between each simulation result of AC, except for the F-UDBC model which performs much better in predicting the local concentration of shear strain. But for the results of the TC condition shown in Fig. 5c, d, the F-UDBC model and the H-PSYBC model can effectively
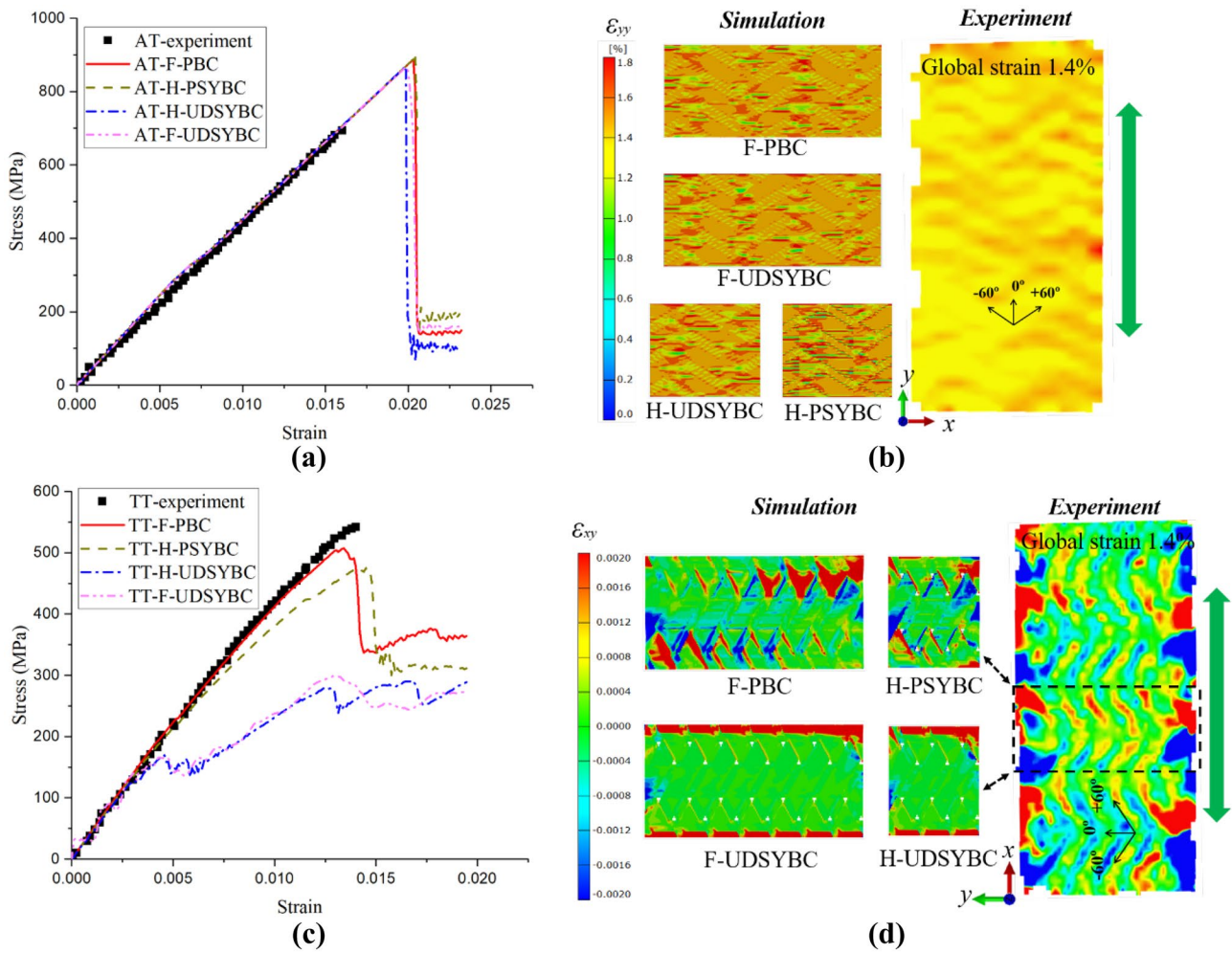
**Fig. 3** Numerical predictions of stress–strain curves and full-field strain distributions under axial tension (**a**, **b**) and transverse tension (**c**, **d**)

capture the distinct antisymmetric deformation field and reasonably predict the ultimate strength. However, in the results of the F-UDSYBC and H-UDSYBC models, the SYBC in the loading edge causes the shear strain concentration and therefore leads to the premature failure of the model.

The accurate simulation of the axial compression should predict the local buckling of fiber tows and the resulting failure behaviors, as shown in Fig. 6a. We can find from Fig. 6a that the F-UDBC model can effectively model the local buckling of axial fiber tows and capture the damage of fiber tows near the grip region. The simulation results of the F-UDSYBC model and the H-UDS-YBC model are comparable in which the damage was concentrated in the loading edge. While employing the PBC through the loading direction in the H-PSYBC model,

the contrived displacement continuity of the nodes in the opposite loading edges produced more uniform damage distributes than that in other models. Furthermore, the SYBC applied on one of the loading edges limits the nodal movement out of the symmetrical plane $\left(U_x^{SYM} = 0\right)$. As a result, the nodes in the two loading edges tend to dispersion and accordingly lead to interface failure near the loading ends, as shown in the lower right corner of Fig. 6a. The results shown in Fig. 6b suggests that the model considering the grip region or employing the PBC along loading direction can generate a pleased result in modeling the transverse compression failure behavior. On the contrary, the models which utilize the SYBC along loading direction drew undesired failure modes on the loading edges and resulted in a tendency to global instability of the model.

**Fig. 4** Comparison of damage patterns predicted by different FE models with the experimental results for the tensile loading conditions: **a** AT and **b** TT
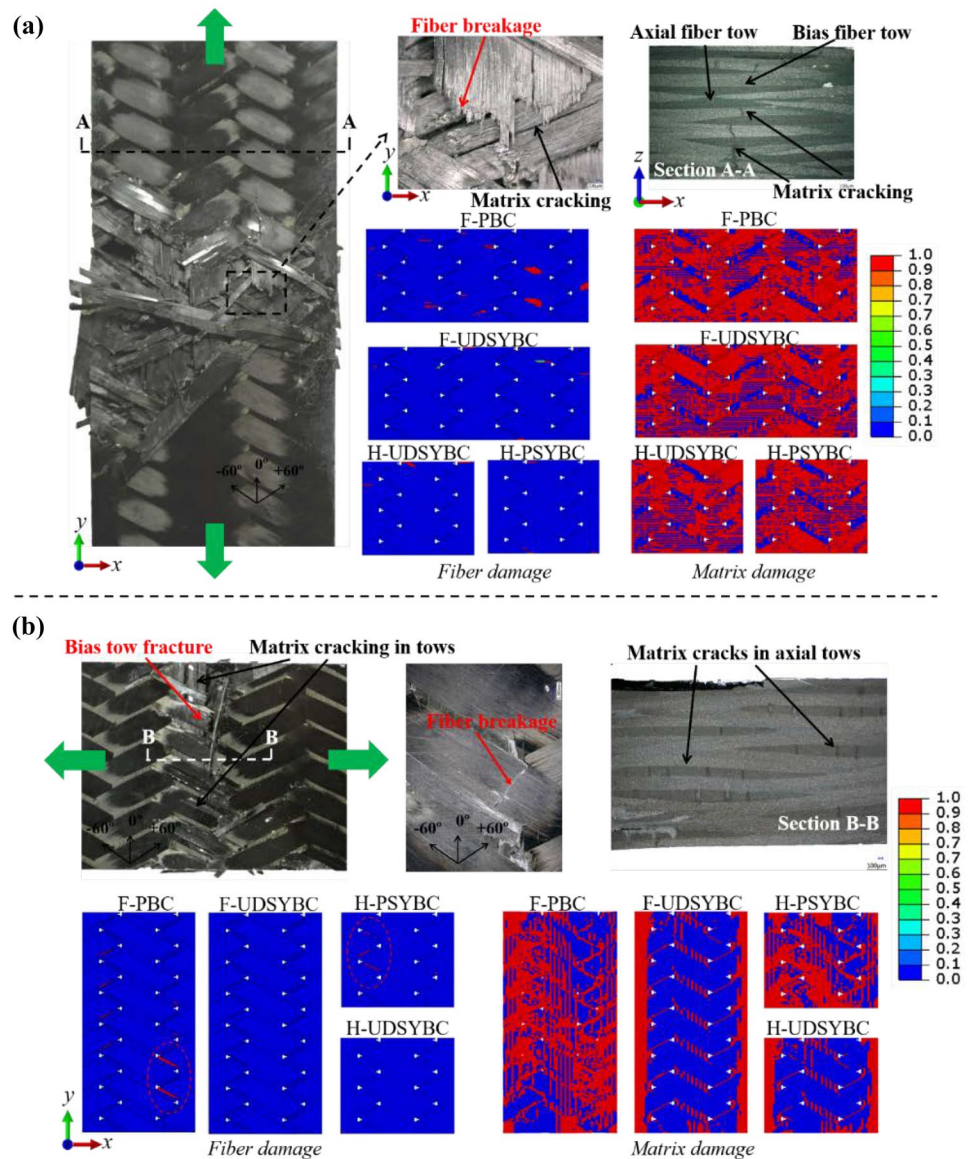


## 3.3 Effect of through-thickness B.C. on the simulation results

This section will discuss the effect of using SYBC or PBC on the thickness direction of the thinner full-width model to simulate the eight-layer coupon specimen. Firstly, the numerical predictions of stress–strain curves using different models are summarized in Fig. 7, and the simulation results from the F-PBC and F-UDBC models are also involved here as indicators. The simulation results of axial tensile and compressive responses from the F-ZSYM and F-ZDSYM models are closed to those of the F-PBC and F-UDBC models. On the contrary, there were significant differences between the results from the F-ZSYM and F-ZDSYM models and the eight-layer

models in predicting the global responses under transverse loading conditions. The predicted strengths, in both transverse tension and transverse compression, increase as constraints are imposed in the thickness direction. In particular, the numerical infinitely thick model (F-ZPBC) predicted the highest value of strength in each loading condition. These results indicate that the model with reduced thickness can maintain accuracy only in predicting the axial mechanical response of an eight-layer 2DTBC coupon specimen. We note that the fluctuation of stress–strain curves at very low-stress levels (see Fig. 7b) is caused by the residual stiffness set to the failure element, which aims to avoid the non-convergence of calculation induced by the element stiffness degradation to 0 in the numerical calculation.
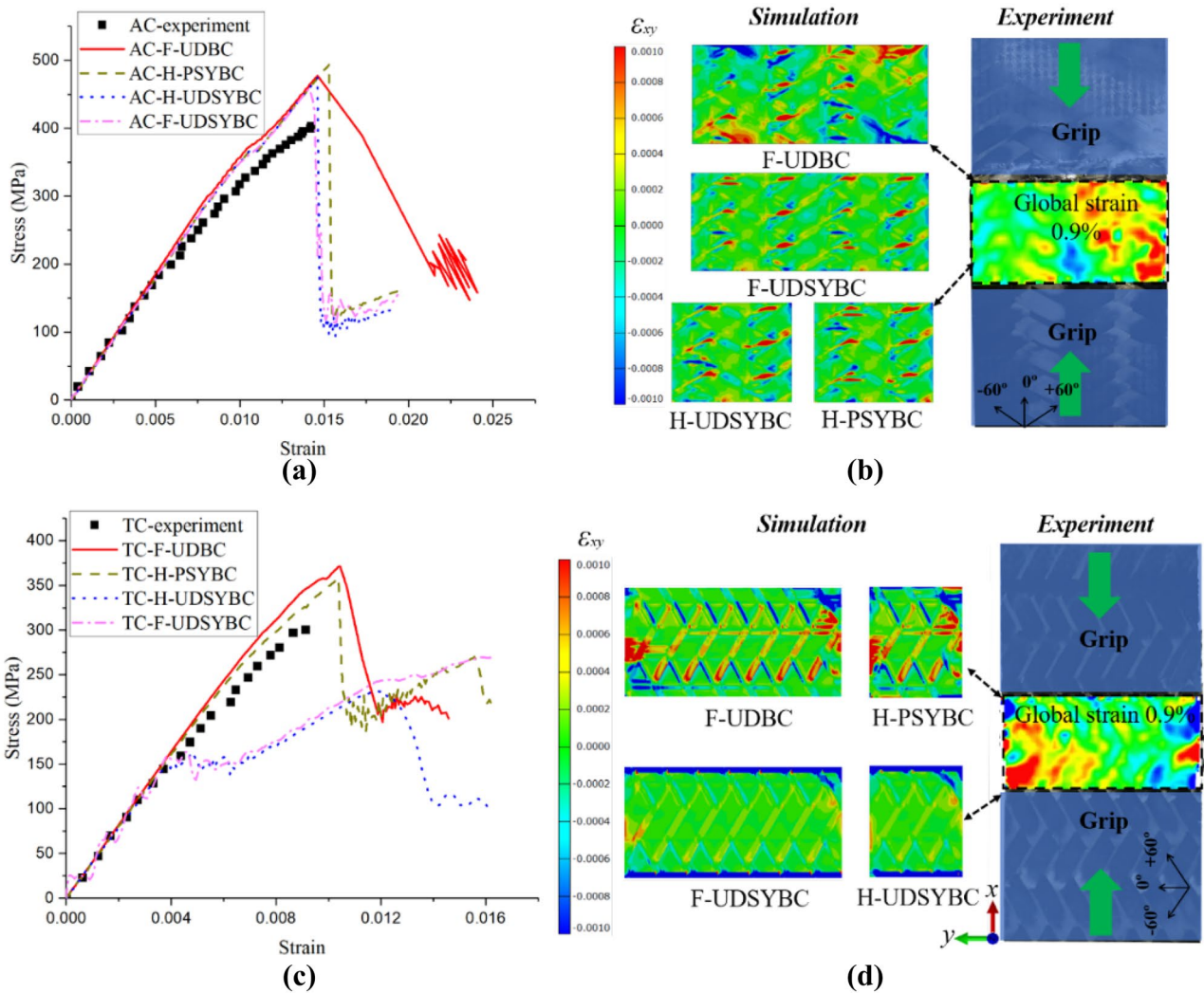
**Fig. 5** Numerical predictions of stress–strain curves and full-field strain distributions under axial compression (**a**, **b**) and transverse compression (**c**, **d**)

Since the results from F-ZSYM, F-ZDSYM, and F-ZPBC models of AT show little difference, the simulated damage patterns of different thick models for transverse loading and the axial compression are further investigated in Fig. 8. From the results of transverse tension and transverse compression, we can see that the patterns of fiber and matrix damages in different models are very similar. However, as the result of axial compression, the imposed unilateral asymmetry in the F-ZSYM model restrained the local buckling of axial fiber tows near the constraint boundary. Hence, the predicted axial compression strength of the F-ZSYM model is a bit higher than the one of the F-UDBC model. In this way, as the constraints are further strengthened in the F-ZDSYM model and F-ZPBC model, out-of-plane deformation, as well as the delamination of the specimen, is forbidden. Consequently, the predicted compression strength is higher than that of the full-size model.

## 3.4 Effect of B.C. on the simulation of the free-edge effect

According to the experimental results in Zhao et al. [40], the transversely tensile and compressive loads will cause significant tension–torsion coupled deformation along the free-edges of the 2DTBC coupon, which is manifested as periodical out-of-plane deformation patterns. Figure 9 compared the out-of-plane deformation contours simulated by all the models aforementioned. From the comparison results, the H-PSYBC model predicted well the antisymmetric out-of-plane warping along the free-edges, which are consistent with the results from F-PBC and F-UDBC models. However, the incorrect deformation field will be obtained if we try to reduce the computation of the FE model by using the symmetric boundary condition in the loading direction or through-thickness direction.

**Fig. 6** Comparison of damage patterns predicted by different FE models with the experimental results for the compressive loading conditions: **a** AC and **b** TC
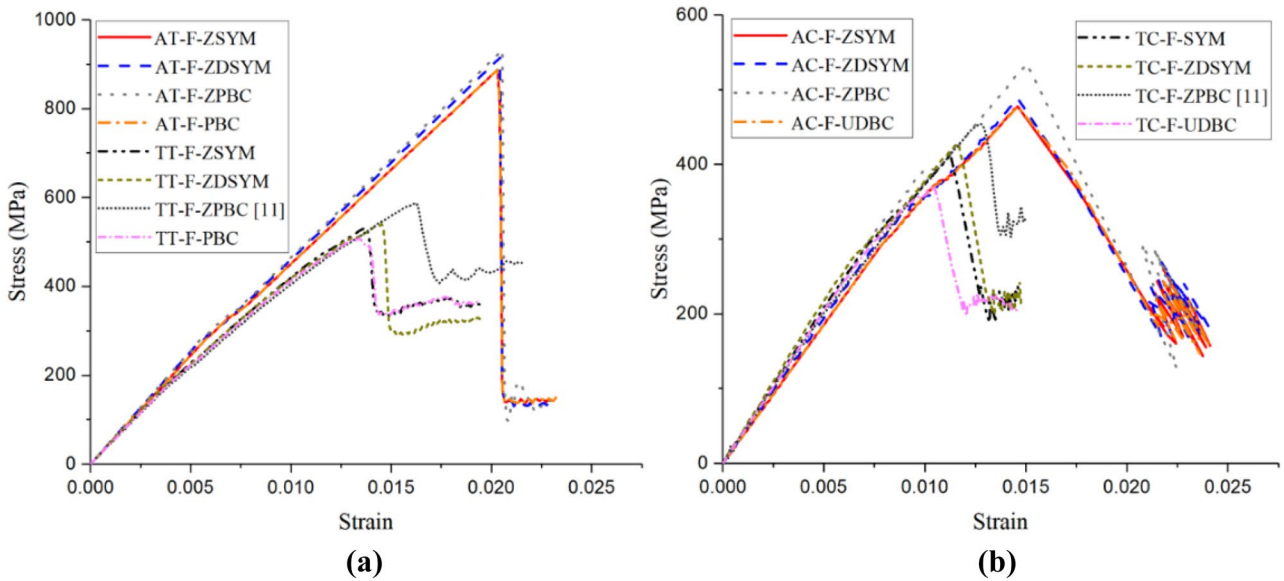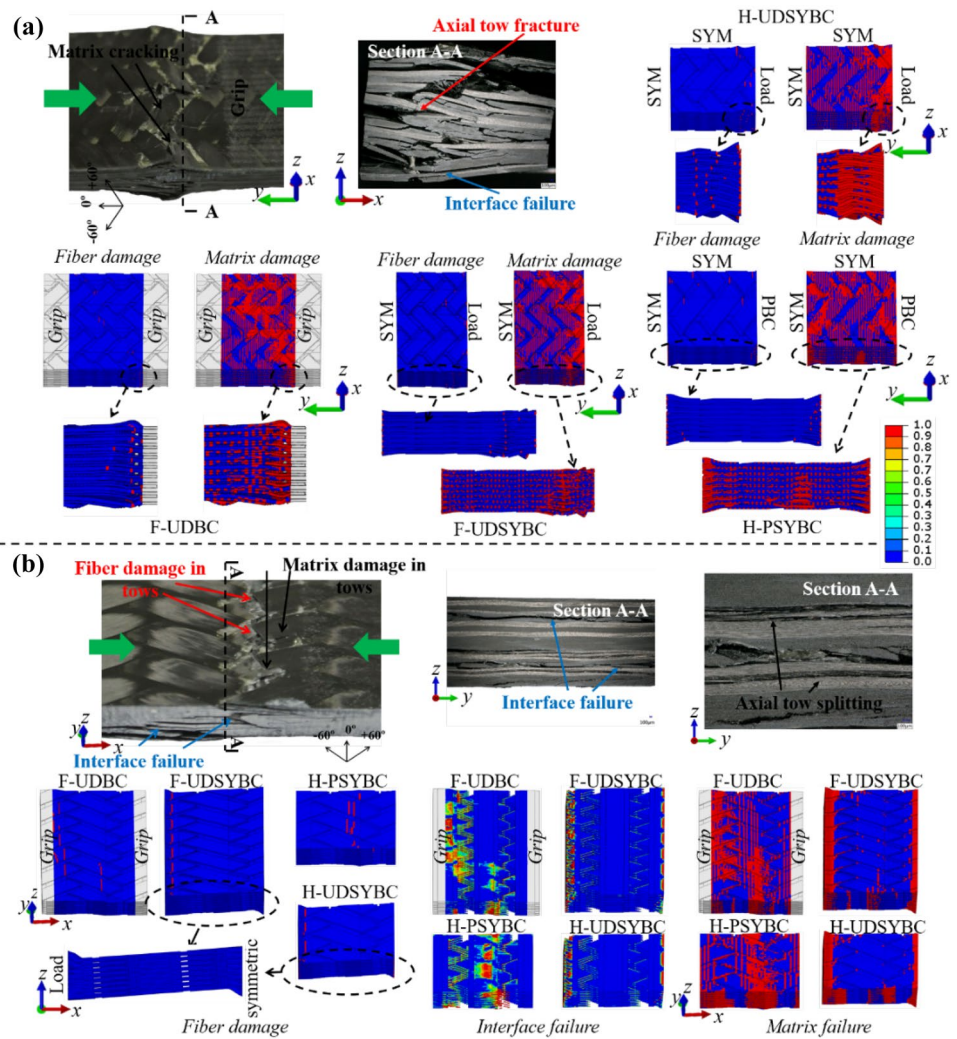


**Fig. 7** Comparison of stress–strain curves predicted by the FE models with different thicknesses for the loadings of **a** axial tension and compression and **b** transverse tension and compression

**Fig. 8** Comparison of numerical predictions of damage patterns from the different thick models
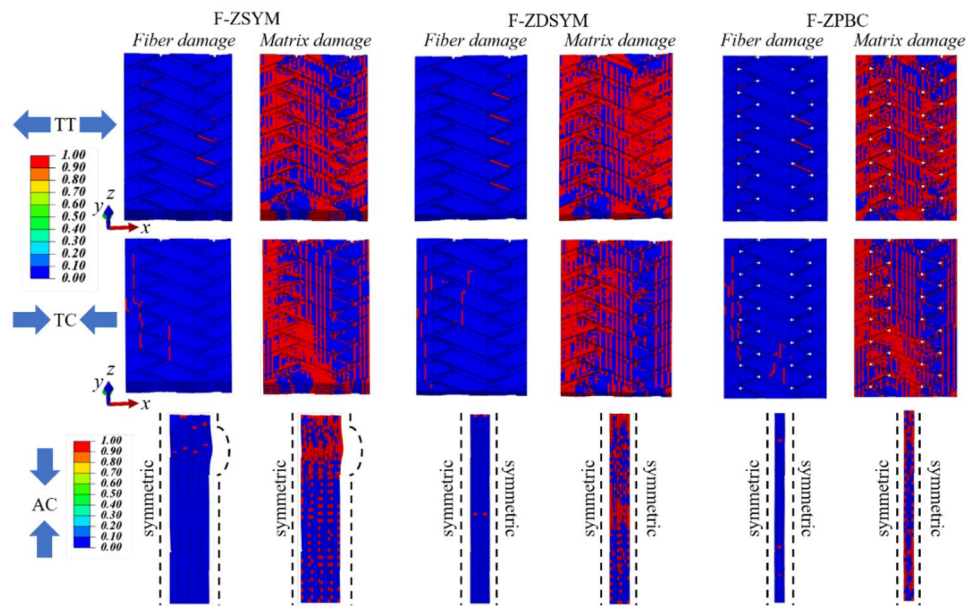


**Fig. 9** Comparison of numerical predictions of out-of-plane deformation patterns from different models under transverse tension and transverse compression
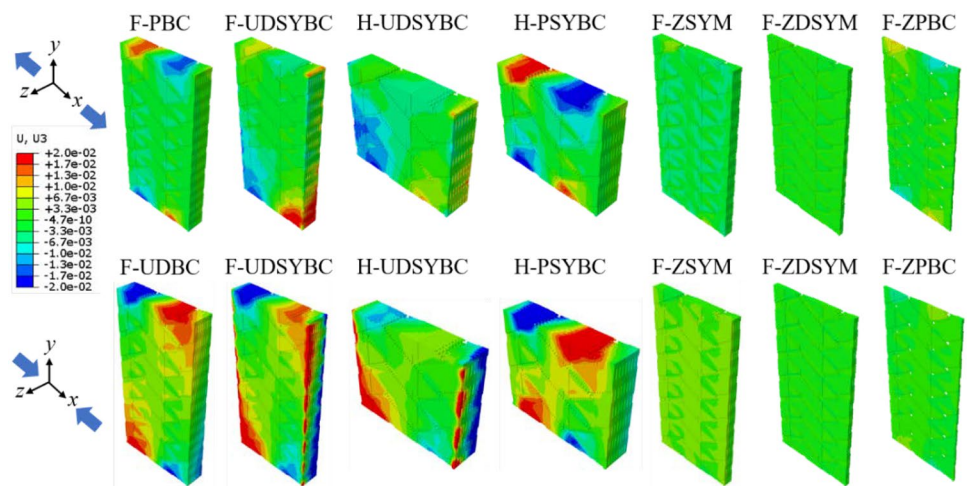


**Table 1** Summary of the modeling capability of different boundary conditions for tensile and compressive simulation of 2DTBC

| Boundary conditions | Tensile simulation | Compressive simulation |
| --- | --- | --- |
| F-PBC | Predicts well the global stress–strain response, and accurately simulates the strain field and the failure morphology | Inapplicable |
| F-UDBC | Inapplicable | Capable of predicting the global stress–strain response, and simulates accurately the strain field and the failure morphology |
| F-UDSYBC and H-UDSYBC | Lead to undesired strain and damage concentration at the loading edges in TT and TC simulations, and deliver poor results in simulating the damage patterns of AC | |
| H-PSYBC | Performing well in simulating the deformation fields and damage patterns under transverse loadings, and the prediction of global stress–strain curves are acceptable | |
| F-ZSYM | Predicts well the global stress–strain response and failure modes, but shows insufficiency in modeling the free-edge effect | Acceptable results in predicting the stress–strain response of AC and the failure modes of TC |
| F-ZDSYM | Capable in modeling the global stress–strain response and failure modes, but shows insufficiency in modeling the free-edge effect | Acceptable results in predicting the stress–strain response of AC and the failure modes of TC |
| F-ZPBC | Similar to F-ZDSYM, the worst simulation results for TT and TC cases | |

# 4 Conclusions

In this study, the applying of boundary conditions in meso-scale FE simulation of the braided composite was systematically analyzed and discussed. Table 1 summarizes the performance of various B.C. for the simulation of different loading conditions. The results provide insights for the development of more effectively meso-FE models of braided composites. The following major conclusions are obtained:

1. The axial-tension simulation results are insensitive to the change of boundary conditions, while the other loading cases show obvious sensitivity to the applied boundary conditions.
2. For transverse tension/compression simulations, the employment of SYBC along the loading direction will cause the undesired strain concentration and premature damage at the loading edges of the specimen, which are different from the experimental situations.
3. Extra constraints along the thickness direction may restrain the normal out-of-plane deformation of the braided composites and thereby cause an overestimation of the transverse strengths.
4. Excluding the stress–strain response, more attention should be paid to the prediction of damage and failure patterns of braided composites, as well as, the major deformation behaviors, including the periodic strain distribution and free-edge out-of-plane deformation.
5. The H-PSYBC is recommended for transverse loading conditions, with good accuracy and computational efficiency (half of the F-PBC and F-UDBC models). Both F-UDSYBC and H-UDSYBC are inadequate for the simulation of transverse loading conditions. The F-ZSYM, F-ZDSYM, and F-ZPBC models present relatively conservative predictions on the mechanical behavior of multi-layered braided composites.

## Declarations

## References

1. Abtew MA, Boussu F, Bruniaux P et al (2019) Ballistic impact mechanisms—a review on textiles and fibre-reinforced composites impact responses. Compos Struct 223:110966
2. Luinge H, Warnet LL (2020) On an application of multi-material composite laminates in the aerospace sector. Adv Compos Hybrid Mater 3:294–302
3. Sun K, Qin J, Wang Z et al (2020) Polyvinyl alcohol/carbon fibers composites with tunable negative permittivity behavior. Surf Interfaces 21:100735
4. Xie P, Liu Y, Feng M et al (2021) Hierarchically porous Co/C nanocomposites for ultralight high-performance microwave absorption. Adv Compos Hybrid Mater 4:173–185
5. Wang Z, Sun K, Xie P et al (2020) Low-loss and temperature-stable negative permittivity in La0.5Sr0.5MnO3 ceramics. J Eur Ceram Soc 40(5):1917–1921
6. Fan W, Shan C, Guo H et al (2019) Dual-gradient enabled ultrafast biomimetic snapping of hydrogel materials. Sci Adv 5(4):eaav7174
7. Das TK, Ghosh P, Das NC (2019) Preparation, development, outcomes, and application versatility of carbon fiber-based polymer composites: a review. Adv Compos Hybrid Mat 2:214–233
8. Ma J, Li Z, Xue Y et al (2020) Novel PEEK/nHA composites fabricated by hot-pressing of 3D braided PEEK matrix. Adv Compos Hybrid Mater 3:156–166
9. Ivanov DS, Baudry F, Broucke BVD et al (2009) Failure analysis of triaxial braided composite. Compos Sci Technol 69(9):1372–1380
10. Cui C, Dong J, Mao X (2019) Effect of braiding angle on progressive failure and fracture mechanism of 3D five-directional carbon/epoxy braided composites under impact compression. Compos Struct 229:111412
11. Lomov SV, Ivanov DS, Verpoest I et al (2007) Meso-FE modelling of textile composites: road map, data flow and algorithms. Compos Sci Technol 67(9):1870–1891
12. De Miguel AG, Pagani A, Carrera E (2019) Free-edge stress fields in generic laminated composites via higher-order kinematics. Compos B Eng 168:375–386
13. Nagaraj MH, Reiner J, Vaziri R, Carrera E, Petrolo M (2020) Progressive damage analysis of composite structures using higher-order layer-wise elements. Compos B Eng 190:107921
14. Chen L, Tao X, Choy C (1999) Mechanical analysis of 3-D braided composites by the finite multiphase element method. Compos Sci Technol 59:2383–2391
15. Li J, Chen L, Zhang Y, Pan N (2011) Microstructure and finite element analysis of 3D five directional braided composites. J Reinf Plast Compos 31(2):107–115
16. Wang C, Zhong Y, Adaikalaraj PF et al (2016) Strength prediction for bi-axial braided composites by a multi-scale modelling approach. J Mater Sci 51:6002–6018
17. Ji X, Khatri AM, Chia ES et al (2014) Multi-scale simulation and finite-element-assisted computation of elastic properties of braided textile reinforced composites. J Compos Mater 48(8):931–949
18. Xiao X, Kia HG, Gong XJ (2011) Strength prediction of a triaxially braided composite. Compos A Appl Sci Manuf 42(8):1000–1006
19. Binienda WK, Li X (2010) Mesomechanical Model for Numerical Study of Two-Dimensional Triaxially Braided Composite. J Eng Mech 136(11):1366–1379

20. Quek SC, Waas AM, Shahwan KW et al (2004) Compressive response and failure of braided textile composites: part 2-computations. Int J Non Linear Mech 39(4):649–663

21. Song S, Waas AM, Shahwan KW et al (2007) Braided textile composites under compressive loads: Modeling the response, strength and degradation. Compos Sci Technol 67(15–16):3059–3070

22. Iarve E, Zhou E, Breitzman T et al (2009) Detailed morphology modeling and residual stress evaluation in tri-axial braided composites. 50th AIAA/ASME/ASCE/AHS/ASC Structures, Structural Dynamics, and Materials Conference, p 2657

23. Nega BF, Woo K (2019) Failure analysis of triaxially braided composite under tension, compression and shear loading. Int J Aeronaut Space Sci 20(2):372–386

24. Tian W, Qi L, Chao X et al (2019) Periodic boundary condition and its numerical implementation algorithm for the evaluation of effective mechanical properties of the composites with complicated micro-structures. Compos B Eng 162:1–10

25. Dong J, Huo N (2016) A two-scale method for predicting the mechanical properties of 3D braided composites with internal defects. Compos Struct 152:1–10

26. Wang X, Wang X, Zhou G et al (2007) Multi-scale analyses of 3d woven composite based on periodicity boundary conditions. J Compos Mater 41(14):1773–1788

27. Zhai J, Zeng T, Xu G et al (2017) A multi-scale finite element method for failure analysis of three-dimensional braided composite structures. Composites 110B:476–486

28. Tian Z, Yan Y, Li J et al (2018) Progressive damage and failure analysis of three-dimensional braided composites subjected to biaxial tension and compression. Compos Struct 185:496–507

29. Cater C, Xiao X, Goldberg RK et al (2015) Experimental and numerical analysis of triaxially braided composites utilizing a modified subcell modeling approach. Proceedings of the American Society for Composites - 30th Technical Conference; Sep. 28–30; East Lansing, MI, United States

30. He C, Ge J, Zhang B et al (2020) A hierarchical multiscale model for the elastic-plastic damage behavior of 3D braided composites at high temperature. Compos Sci Technol 196:108230

31. Kaleel I, Carrera E, Petrolo M (2020) Progressive delamination of laminated composites via 1D models. Compos Struct 235:111799

32. Shen X, Liu X, Dong S et al (2018) RVE model with shape and position defects for predicting mechanical properties of 3D braided CVI-SiC_f/SiC composites. Compos Struct 195:325–334

33. Fu Y, Gao X, Yao X (2020) Mesoscopic simulation on curing deformation and residual stresses of 3D braided composites. Compos Struct 246:112387

34. Chen Y, Yang P, Zhou Y et al (2020) A Micromechanics-based constitutive model for linear viscoelastic particle-reinforced composites. Mech Mater 140:103228

35. Chen Y, Xin L, Liu Y et al (2019) A viscoelastic model for particle-reinforced composites in finite deformations. Appl Math Model 72:499–512

36. Barbero EJ, Lonetti P, Sikkil KK (2006) Finite element continuum damage modeling of plain weave reinforced composites. Compos B Eng 37:137–147

37. Jiang H, Ren Y, Zhang S et al (2018) Multi-scale finite element analysis for tension and ballistic penetration damage characterizations of 2D triaxially braided composite. J Mater Sci 53(14):10071–10094

38. Liu T, Sun B, Gu B (2018) Size effects on compressive behaviors of three-dimensional braided composites under high strain rates. J Compos Mater 52(28):3895–3908

39. Zhang C, Binienda WK, Goldberg RK (2015) Free-edge effect on the effective stiffness of single-layer triaxially braided composite. Compos Sci Technol 107:145–153

40. Zhao Z, Liu P, Chen C et al (2019) Modeling the transverse tensile and compressive failure behavior of triaxially braided composites. Compos Sci Technol 172:96–107

41. Kueh AB (2014) Size-influenced mechanical isotropy of singly-plied triaxially woven fabric composites. Compos A Appl Sci Manuf 57:76–87

42. Gupta US, Dhamarikar M, Dharkar A et al (2020) Study on the effects of fibre volume percentage on banana-reinforced epoxy composite by finite element method. Adv Compos Hybrid Mater 3:530–540

43. Song S (2007) Compression response of tri-axially braided textile composites. PhD thesis, The University of Michigan, Ann Arbor

44. Zhang C, Curiel-Sosa JL, Bui TQ (2017) Comparison of periodic mesh and free mesh on the mechanical properties prediction of 3D braided composites. Compos Struct 159:667–676

45. Hashin Z (1980) Failure Criteria for Unidirectional Fiber Composites. J Appl Mech 47(2):329–334

46. Bažant ZP, Oh BH (1983) Crack band theory for fracture of concrete. Mater Struct 16(3):155–177

47. Zhao Z, Zhang C, Li Y (2018) Tensile and compressive failure behaviors of triaxially braided composite. Proceeding of American Society for Composites 33rd Technical Conference; Sep. 24–27; Seattle, WA, United States

48. Li X, Binienda WK, Goldberg RK (2011) Finite-element model for failure study of two-dimensional triaxially braided composite. J Aerosp Eng 24(2):171–180